Structural Engineering of Cyanine Dyes to Access Highly Redshifted and Emissive J-aggregates

Jillian A. Williams,[†a] Austin D. Bailey,[†a] Monica Pengshung,[a] Arundhati P. Deshmukh,[a] Cesar Garcia,[a] John Cao,[a] Barry Y. Li,[a] Nadine C. Bradbury,[a] Alexandra Wright,[a] Chern Chuang,[b] Daniel Neuhauser,[a] Ellen M. Sletten,[a] and Justin R. Caram*[a]*

Department of Chemistry & Biochemistry, University of California Los Angeles, Los Angeles, CA 90024

[†] These authors contributed equally.

Abstract

Molecular design of two-dimensional (2D) and tubular excitonic aggregates would enable access to extraordinary and unusual photophysical properties via control over supramolecular structure. Here, we synthesize four heptamethine cyanines that enable a rational investigation of the role of steric bulk on aggregate self-assembly, morphology and photophysics. Despite near identical monomer photophysics, minute changes to structure and solvation lead to extreme differences in resultant J-aggregate morphology and photophysics. Additional steric bulk not only redshifts aggregate absorption, but also alters the kinetics/thermodynamics of self-assembly, yielding a variety of connected morphological supramolecular phases. We employ cryo-electron and atomic force microscopy, dynamic light scattering and computational screening to characterize 3-4 2D/tubular J-aggregates for each dye, enabling us to predict the monomer packing arrangements. Differentiating and tuning each unique morphology demonstrates approaches to structurally engineer highly redshifted molecular 2D molecular aggregates via synthetic design, achieving extramolecular control over their photophysics.

Introduction

Fluorescence in the near- and shortwave infrared regions of the electromagnetic spectrum (NIR, 700–1000 nm; SWIR, 1000–2000 nm) enables enhanced sensitivity and detection through complex media such as biological tissue. Consequently, developing emissive materials for these regions has become a significant area of research. Polymethine fluorophores have emerged as favorable contrast agents for the NIR and SWIR regions due to their non-toxicity, spectral tunability, and excellent absorption properties.[1–5] We and others have capitalized on the beneficial properties of polymethine fluorophores to perform multiplexed non-invasive imaging.[6–13] Additional applications in photovoltaics,[14–17] opto-electronic applications,[18–20] and polaritonics[21–23] make these fluorophores valuable chemical tools.

An avenue to further advance the photophysical properties of polymethine fluorophores is to engineer their aggregation to form J-aggregates (Figure 1a). J-aggregates are bathochromically shifted compared to the parent monomeric fluorophores and display increased peak absorptivity (ϵ_{max}) (due to peak narrowing) and often increased radiative rates (k_r).[24–26] This is in contrast to the typical H-aggregation observed for polymethine fluorophores that result in broad, hypsochromically-shifted absorption and quenched emission. While J-aggregates display favorable photophysical properties, systematic methods to promote J-aggregation (and prohibit H-aggregation) are limited, particularly for NIR and SWIR fluorophores. Previous studies have investigated a broad selection of dyes, but they seldom focus on the effects of one particular modification.[27] Recent research has shown how modifications to the heterocycles[6,28] or central position of polymethine dyes affect the resulting aggregate photophysics,[29,30] but additional research is necessary to elucidate the connection between monomer structure and aggregate photophysics and inform the rational design of new dyes.

An added complexity of J-aggregation is that their supramolecular structure can significantly alter the photophysical properties as the larger 2D assemblies dictate short- and long-range order and coupling.[3,4] 2D aggregates are unique as they often display large redshifts (~2,000-3,000 cm^{-1}), increased exciton delocalization, bigger changes in radiative rates, narrower absorption linewidths and longer-range energy transfer compared to their one-dimensional counterparts.[24,31,32] These enhanced properties arise from the high transition dipole moments and denser packing availed by 2D and tubular chromophore arrangements. Cyanine dyes within the visible region have been characterized to form a wide-range of geometries including namely, sheet-like aggregates, double and single-walled nanotubes, bundles of tubes, and ribbonlike aggregates.[5–7,33] For NIR and SWIR aggregating polymethine dyes, only sheet and ribbon-like structures have been reported to date. Accessing tubular structures may result in enhanced photophysical properties owing to their mixed 1D/2D character.[34,35] More broadly, general design principles for achieving emissive infrared J-aggregates would facilitate their use in diagnostics, sensors, and other optically active materials.

A majority of J-aggregation studies on polymethine dyes are performed on commercially available fluorophores. While this work has revealed distinct J-aggregate structures and facilitated the study of conditions that affect their assembly, it has not allowed for subtle structural features of the dyes to be probed. Previous work has established that the slip parameter, or the offset between neighboring monomer dyes, is directly related to the location of the bright state within the density of states, in which a larger slip pushes the bright state toward the lower band edge.[36] We hypothesized that by introducing increasingly bulky groups in the central 4’ position would result in an increase in slip, leading to a more redshifted J-aggregate.

Here, we report a series of dyes that vary in the steric bulk of their pendant group (4' substitution, Figure 1b): phenyl (**1a**), 3,5-dimethylphenyl (**1b**), 3,5-diethylphenyl (**1c**), and 3,5-

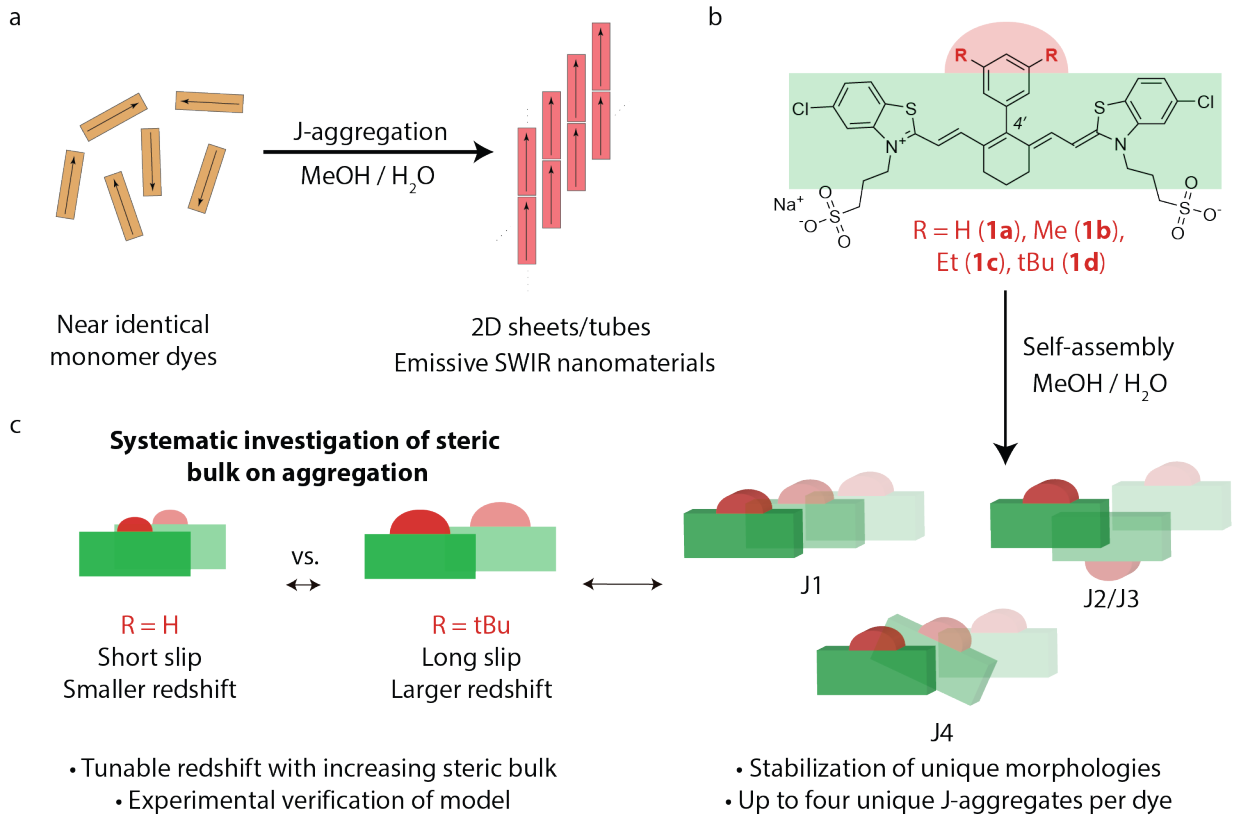

Figure 1. a) Cartoon representing self-assembly of dye monomers upon J-aggregation. **b)** Molecular structure of heptamethine cyanine dyes studied in this work and proposed J-aggregate morphological phases. **c)** Predicted effects of sterics on packing parameters of J-aggregation.

ditertbutylphenyl (**1d**). The introduction of steric bulk at the 4' position using aryl group substitutions was specifically chosen to limit changes in solubility or electronic states of the dye monomer. *Each dye was screened for aggregate formation, revealing a surprising number of complex and connected NIR/SWIR J-aggregate mesophase with distinct photophysical properties, despite deriving from highly similar fluorophores with near identical photophysical properties in ethanol.*

We demonstrate that increased steric bulk does result in more redshifted aggregates, confirming our original hypotheses. We further extensively characterize nearly all the supramolecular assembly of these aggregates via cryogenic transmission electron microscopy, atomic force microscopy, and dynamic light scattering to understand the differences between the J-aggregate structures that can be obtained from a single fluorophore. We identify the first tubular shortwave infrared J-aggregate, a single-walled structure which shows clear parallel and perpendicular transitions, a system which may enable directional energy transport and polarized absorption and emission.

These findings are reported in four sections. In section 1, we describe the synthesis and screening of these aggregates which enabled us to observe and isolate all J-aggregated mesophases for **1a-d**. In section 2, we discuss the analysis of the "J1" aggregate, which we assign to cofacial packing of monomers, illustrating how steric bulk ultimately redshifts the resultant aggregates in a manner consistent with computation. In section 3, we focus on the four aggregates derived from chromophore **1b**, which show an enormous range in photophysical properties via minimal changes in solvation conditions. We characterize each aggregate via TEM and AFM and probe how the different J-aggregate mesophases connect to each other, allowing us to hypothesize potential unit cell structures and tubular geometries. Finally, in section 4 we connect these assignments to a description to the structure of all aggregates derived from **1a-1d**.

Results and Discussion

1. Synthesis and Aggregate Screening of Isoelectronic Cy7 Benzothiazole Dyes: Benzathiaozole heptamethine dyes **1a-d** (Figure 2a) were synthesized in two steps. First, Suzuki coupling of linker **2** containing a vinyl chloride with aryl boronic acids bearing the various steric

substituents (**3a-d**) provided electrophilic linkers with varying steric bulk **4a-d**. These linkers were then reacted with heterocycle **5** in the presence of base to yield **1a-d** in 9–54% yield.

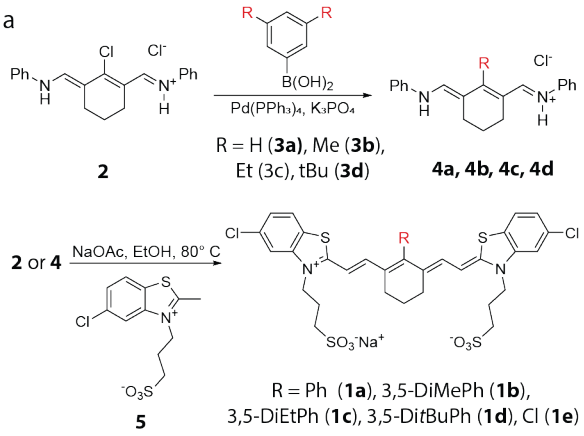

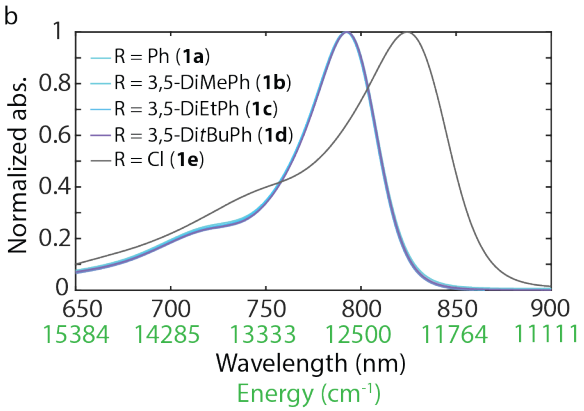

c

Dye	λ_{abs} (nm)	λ_{em} (nm)	ε (x 10^5 $M^{-1}cm^{-1}$)	Φ_F (%)
1a	798	813	1.62 ± 0.08	5.2 ± 0.2
1b	798	814	1.80 ± 0.05	6.6 ± 0.4
1c	798	812	2.12 ± 0.05	5.1 ± 0.2
1d	798	813	1.93 ± 0.04	6.7 ± 0.6
1e	828	834	0.15 ± 0.01	0.57 ± 0.1

Figure 2. a) Monomer synthesis of sterically hindered cyanines **1a-e**. **b)** Absorption spectra for **1a-e** monomers in ethanol. **c)** Tabulated monomer dye photophysics in ethanol.

We characterized the photophysical properties of the unaggregated heptamethine dyes **1a-d** in ethanol where they were readily solubilized. We found that the monomers all share near identical absorption (798 nm) and emission (~813 nm) wavelengths (Figure 2b), as well as similar molar absorptivity (ε) and fluorescence quantum yield (Φ_F) (Figure 2c), demonstrating that the different alkyl chains are not affecting the electronics of the fluorophores.

Next, we surveyed the aggregation landscape of each dye. In stark contrast to the parent monomeric dyes, we observed distinct differences in the aggregation of **1a–d** when introducing them to methanol: water mixtures, supporting our hypothesis that the 4' substituents could modulate the resultant aggregate. What was unexpected was the degree of complexity observed in these initial aggregate screens where multiple red-shifted species were observed for each fluorophore. To isolate each of the individual J-aggregates, we first prepared 20% (v/v) methanol/water samples with dye concentrations 0.01, 0.1 and 1 mM (Figure S1a). Next, we

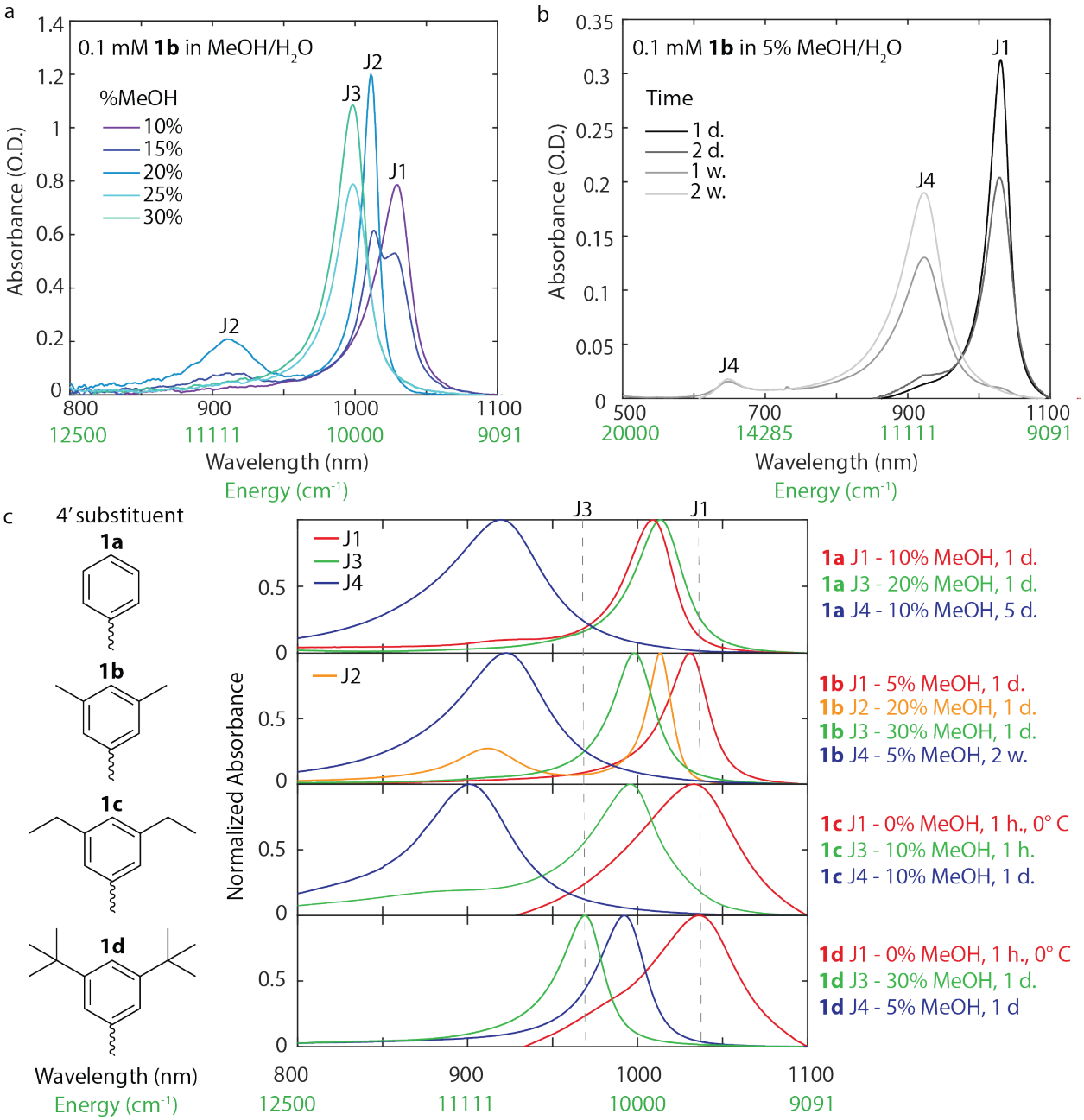

Figure 3. a) Absorption screening of 0.1 mM **1b** in different MeOH/H2O composition solutions after 24 h. **b)** Kinetic absorption screening of 0.1 mM 5b in 5% MeOH/H2O **1b** after different timepoints. **c)** Isolated aggregate absorption for J1, J2, J3, and J4 of **1a-d**

prepared 0.1 mM dye solutions with methanol/water composition that varied from 0 to 40% in 5-10% increments (Figure 3a, Figure S1b). We then performed time-course studies for each aggregate at selected methanol percentages (Figure 3b, Figure S1b-c). Lastly, we prepared 0% methanol/water samples at 0°C to isolate the **1c** and **1d** J1 aggregates.

Through these screening procedures, we observed that the dyes form a minimum of three unique aggregates which can be isolated with some combination of methanol/water ratio, time, and temperature. We enumerate the J-aggregates as J1, J2, J3, and J4 based on their physical characterizations and self-assembly conditions (*vide infra*). In short, J1 represents the aggregates formed at low (~5%) methanol and short times, J2 is a special case only forming from **1b** at 20% methanol, J3 is stable at higher (~30%) methanol, and J4 is the slower-forming product from J1 aggregates (~5% methanol) over extended times (1-2 weeks). Figure 3c displays the normalized absorption of each isolated aggregate from dyes **1a-d** which represent the best conditions for forming that specific aggregate from the systematic solvation, time, temperature screens. This abundance of J-aggregates obtained from a single monomer is highly unusual among polymethine dyes, where 1-2 unique J-aggregates are typically identified.[5] We believe **1b** is the first example of a single cyanine chromophore aggregating to form up to four distinct spectra that can be isolated at room temperature.

The photophysical properties of these aggregates are presented in Table 1. We observe that the J1 analogues experience a redshift as the steric bulk of the monomer is increased, while the J3 analogues experience a blue-shift. We hypothesize these trends are related directly to the distinct monomer packing that differentiates the aggregates and will explore this in more detail shortly. The **1a** J4 and the **1b** J2 and J4 aggregates each exhibited two distinct spectral peaks, while the remaining dyes only produced one. The appearance of a second peak indicates some out-of-plane bright state, which will be further discussed with the characterization of the aggregates. The relative quantum yields obtained for the J1 aggregates were all negligibly similar (0.02-0.03%), while the **1d** J4 aggregate had the largest quantum yield collected at 0.08%.

Table 1. Aggregate photophysics for redshifted morphologies of the **1a-1d** aggregates.

Dye	Aggregate	$\lambda_{max,abs}$	$\lambda_{max,em}$	$\Phi_{relative}$ (± 0.01%)
1a	J1	1004	1009	0.03%
1a	J3	1012	1027	0.05%
1a	J4	921		
1b	J1	1029	1049	0.03%
1b	J2	1011 +910	1027	0.02%
1b	J3	998	1010	0.05%
1b	J4	923 + 649		not emissive
1c	J1	1032	1043	0.02%
1c	J3	996		
1c	J4	900		
1d	J1	1034	1050	0.02%
1d	J3	965	991	0.08%
1d	J4	990	995	

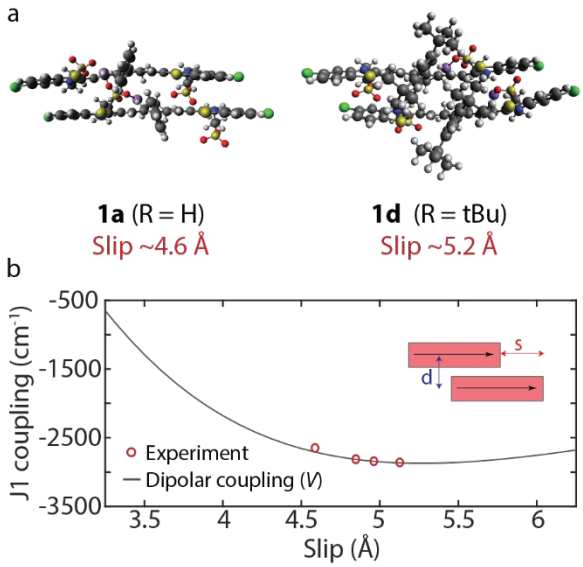

Figure 4. **a)** Model of **1a** and **1d** with optimized slip values between neighboring monomers. **b)** Relationship between slip and J-coupling responsible for dye redshifting.

2. Computational Analysis: To further quantify the effects of steric bulk on the redshift observed for the J1 analogues of the **1a-1d** dyes, we employed a computational approach that allowed us to estimate the relative slip for a given 4' substitution. We used density functional theory (DFT) method to optimize the ground state geometries of each dye (**1a-d**) in a dimer arrangement, then calculated energies of those dimers as they are slipped across each other from a distance of 1 to 7 Å. We observed a trend that as steric bulk increased (i.e. from **1a** to **1d**), the slip that produces the lowest energy for the dimers increased, visualized in Figure 4a. Because previous reports have shown that the dye-to-dye slip

increases with number of monomer units, we added 2 Å of slip to each estimate to compensate for the dimeric limit[37], allowing us to plot the redshift for J1 aggregates of **1a-d** as a function of their slip (steric bulk) in Figure 4b. The slip was then compared to a model of in-plane dipole coupling (Equation 1)

$$J = \frac{\mu^2(d^2-2s^2)}{||d^2+s^2||^{\frac{5}{2}}} \quad (1)$$

where J is the coupling strength, μ is the transition dipole moment (μ = 1063 D), d is the distance between neighboring bricks (d = 4.302 Å), and s is the slip, which refers to the offset between neighboring bricks (Figure 4b). The correlation between the slip and the J-coupling allows us to draw a direct relationship between the chromophore packing parameters and the resulting photophysical properties, resulting in an estimated slip of 4.6 Å for the least-sterically-hindered **1a** J1 aggregate and an estimated slip of 5.2 Å for the most-sterically hindered **1d** J1 aggregate. These results support our hypothesis that the size of the central group can induce a larger slip between neighboring monomers, leading to a redshift in the aggregate's optical properties. This is consistent with our prior results that suggest relative slip can be used to tune the short-range coupling contributions, and thus the resulting excitonic band structures.[3,24]

3. Characterization of J-aggregate Mesophases: With the unprecedented finding that benzothiazole heptamethine dye **1b** readily formed four different J-aggregates, we aimed to understand the supramolecular differences of all structures using a combination of CryoEM and AFM (Figure 5). In figure 5a, we focus on J1-J4 of **1b**. CryoEM was employed to view the native morphologies of each aggregate (J1-J4) of **1b**. The J1, J3, and J4 aggregates were all found to have a sheet-like 2D morphology. However, the J2 aggregate of **1b** was anomalous, consisting of micron-scale single-walled nanotubes measuring ~ 5 nm in diameter (Figure 5a). Imaging

performed on the aggregates of the remaining dyes (**1a**, **1c**, **1d**) also shows 2D structures (Figure S2). The J1 aggregate of the **1c** and **1d** dyes and the J3 aggregate of the **1c** dyes were unable to be isolated for imaging but based on the single-peak lineshapes observed in the absorption spectra, it

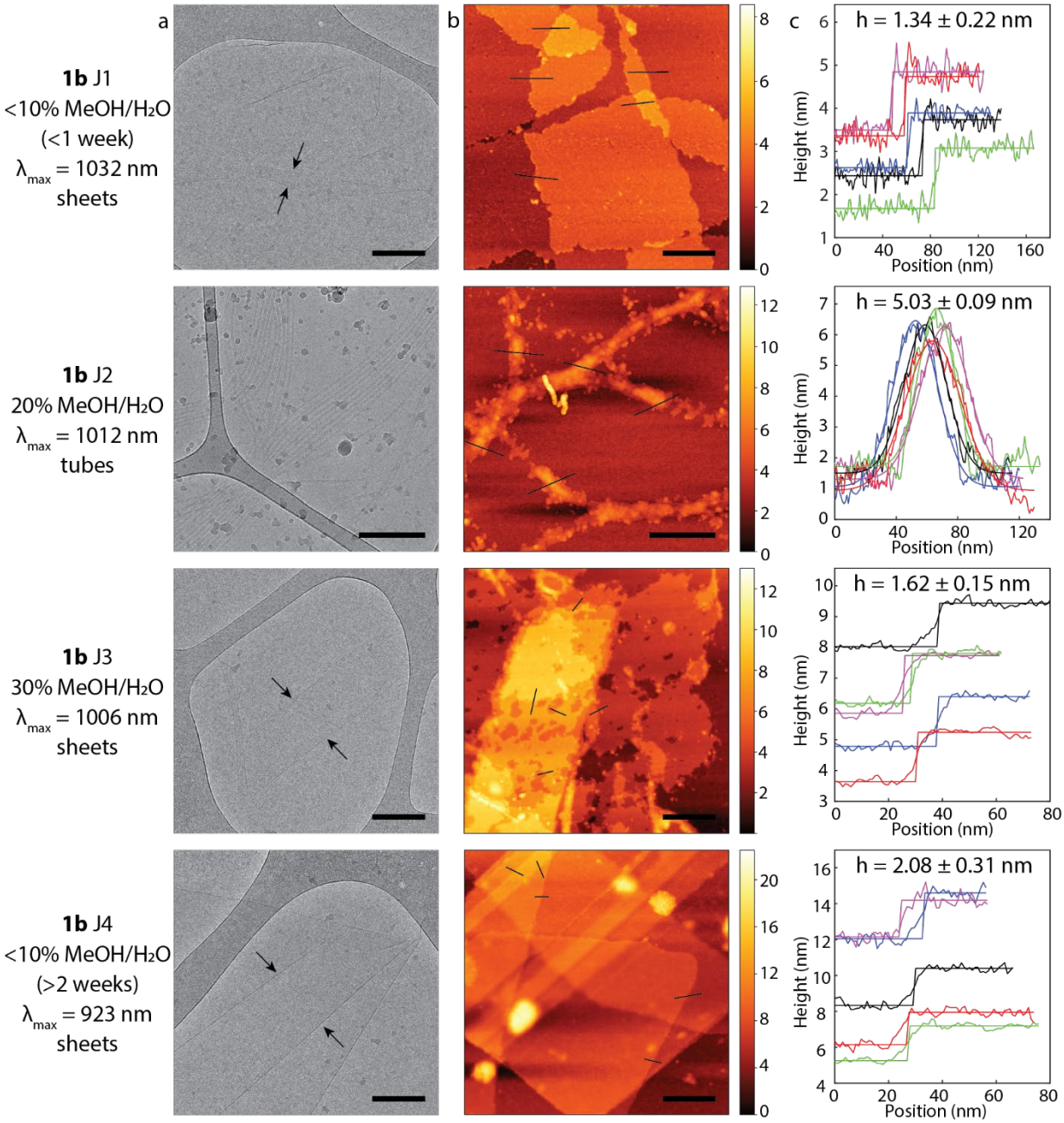

Figure 5. a) CryoEM images of J1-J4 aggregates of dye **1b,** showing sheetlike morphologies for J1, J3 and J4 and a tubelike structure for J2. **b**) AFM images of J1-J4 aggregates of dye **1b,** with color bars presenting height in nm. **c**) Height profiles were extracted from the indicated regions on the AFM images and fit to determine the average height differences between layers of sheets. All scale bars are 200 nm.

is most likely that these dyes also produce 2D sheet-like structures. These results indicate that **1b** dye is the only dye which allows formation of the tubular J2 aggregate.

Although the J1, J3 and J4 aggregates share a similar sheet-like morphology, the packing geometries of these aggregates must be distinctly different to produce absorption energies that vary by up to 100 nm (from ~1000nm to 900nm or 1,000 cm^{-1}). This indicates that a single cyanine dye can self-aggregate to form three distinct packing geometries—with distinct photophysical properties—that can be controlled via solvent. The similar morphologies associated with these aggregates makes elucidating the differences in the packing geometries a challenge. Traditional techniques for solving mesoscale structures, such as x-ray scattering, are not applicable here due to low periodic order and the lack of long-range symmetry elements preventing crystallization. Instead, we employ several experimental techniques (AFM, DLS, and kinetic experiments) to gain additional information on the morphological phases.

In order to determine the heights of the structure, AFM images were also obtained for all aggregates that could be isolated. Figure 5b shows the AFM images of the **1b** dye aggregates J1-4, respectively, along with the fitting used to extract the heights of the aggregates. The heights of all the aggregates measured via AFM are presented in Table 2 and Figure S3. The diameter of the tubular J-aggregate is measured at 5.03 nm, which is consistent with the diameter estimated by cryo-EM. The heights of the sheet-like aggregates range from 1.34 to 2.08 nm where J1 < J3 < J4 holds true for **1a** and **1b**. In the case of **1d**, the aggregate heights followed the trend J1 < J4 < J3. These heights are consistent with a single monomer height for each dye, and we hypothesize that the changes in the aggregate dye heights are caused by out-of-plane or alternating orientations of the monomer within the aggregate structure. In section 4, we will elaborate on how this preliminary

structural assignment is consistent with observed spectroscopic changes between different chromophores.

In addition to those characterizations, we employed dynamic light scattering (DLS) to get a relative estimate of the aggregate size in solution. Our DLS analysis revealed general patterns, namely that the J1 aggregates appeared smaller than their J3 and J4 counterparts across dyes **1a** and **1b**. The aggregates of **1c**, which were too small to see by cryo-EM, also appeared smaller than others by DLS. Because DLS is not intended for extended sheet structures, we cautiously report one significant digit for each aggregate's size, as a tool to generally classify large size differences, in contrast to the more precise sizing from cryoEM and AFM. Table 2 shows that systematic trends exist between the J1, J3, and J4 aggregates of dyes **1a-d** in solution and that our structural characterizations are consistent across the various dyes.

Table 2. Structural information for all aggregates based on AFM and DLS. Aggregates that could not be fully isolated for characterization are marked with an asterisk.

Dye	Aggregate	Morphology	AFM thickness (nm)	DLS Size (nm)
1a	J1	Sheets	1.24 ± 0.38	300
1a	J3	Sheets	1.24 ± 0.30	400
1a	J4	Sheets	2.11 ± 0.36	700
1b	J1	Sheets	1.34 ± 0.22	200
1b	J2	Tubes	5.03 ± 0.09	200
1b	J3	Sheets	1.62 ± 0.15	600
1b	J4	Sheets	2.08 ± 0.31	600
1c	J1	*	*	*
1c	J3	*	*	*
1c	J4	Sheets	1.56 ± 0.34	300
1d	J1	*	*	*
1d	J3	Sheets	2.89 ± 0.29	600
1d	J4	Sheets	1.54 ± 0.31	600

3.1 Characterization of Tubular Aggregate: Upon learning that **1b** possesses a tubular morphology (J2), we employed linear dichroism (LD) to further characterize these aggregates

(Figure S4). The information from these spectra allowed us to model the tubes and extract their chiral angle using a Frenkel exciton Hamiltonian (Equation 2).

$$H = \sum_{n,m}^{\square} [J_{nm}|n\rangle\langle m| + \text{H. c.}] \tag{2}$$

Here J_{nm} is the exciton coupling strength, $|n\rangle$ represents the state where the nth dye is in its electronic excited state with all others in the ground state. We adopt a stacked-ring description for the tubular aggregates in question. Two bright states were identified for the tubular aggregate, one polarized parallel and the other polarized perpendicular to the cylindrical symmetry axis. The energy gap between these states is represented by Equation 3.

$$\Delta E = E_{\perp} - E_{\parallel} \approx \frac{1}{4\pi\epsilon_0} \cdot \frac{2\pi\mu_0^2}{r\, A_0} \sin^2\theta \tag{3}$$

Here r is the tube radius, A_0 is the area of each molecular site projected onto the tube surface, and θ is the angle between the transition dipole moment and the cylindrical axis. With this information, we are able to estimate chiral angle θ = 43.5 deg for these tubular structures (see supporting information section # for full analysis).

3.2 Kinetics and thermodynamics of **1b** dye assembly**:** Lastly, we performed a thorough investigation of the kinetics of the aggregates derived from **1b** to rationalize the conversion among J1, J2, J3, and J4 morphologies. We rapidly took absorbance spectra (every ~30 s.) immediately upon mixing the dye stock solution with water for a period of at least 10 minutes. We then continued collecting spectra at shorter timepoints (every 10 min. to every 2 h.) to carefully watch the self-assembly unfold. The absorption spectra from initial and extended timepoints are presented in Figure 6a.

Figure 6a shows that the **1b** J1 (0-15% MeOH) initializes with a small amount of H-aggregate (~600 nm), which becomes much less prominent after 1 hour. Depending on the %MeOH content of the solution, the J1 will interconvert to J4 over time, with higher percentages

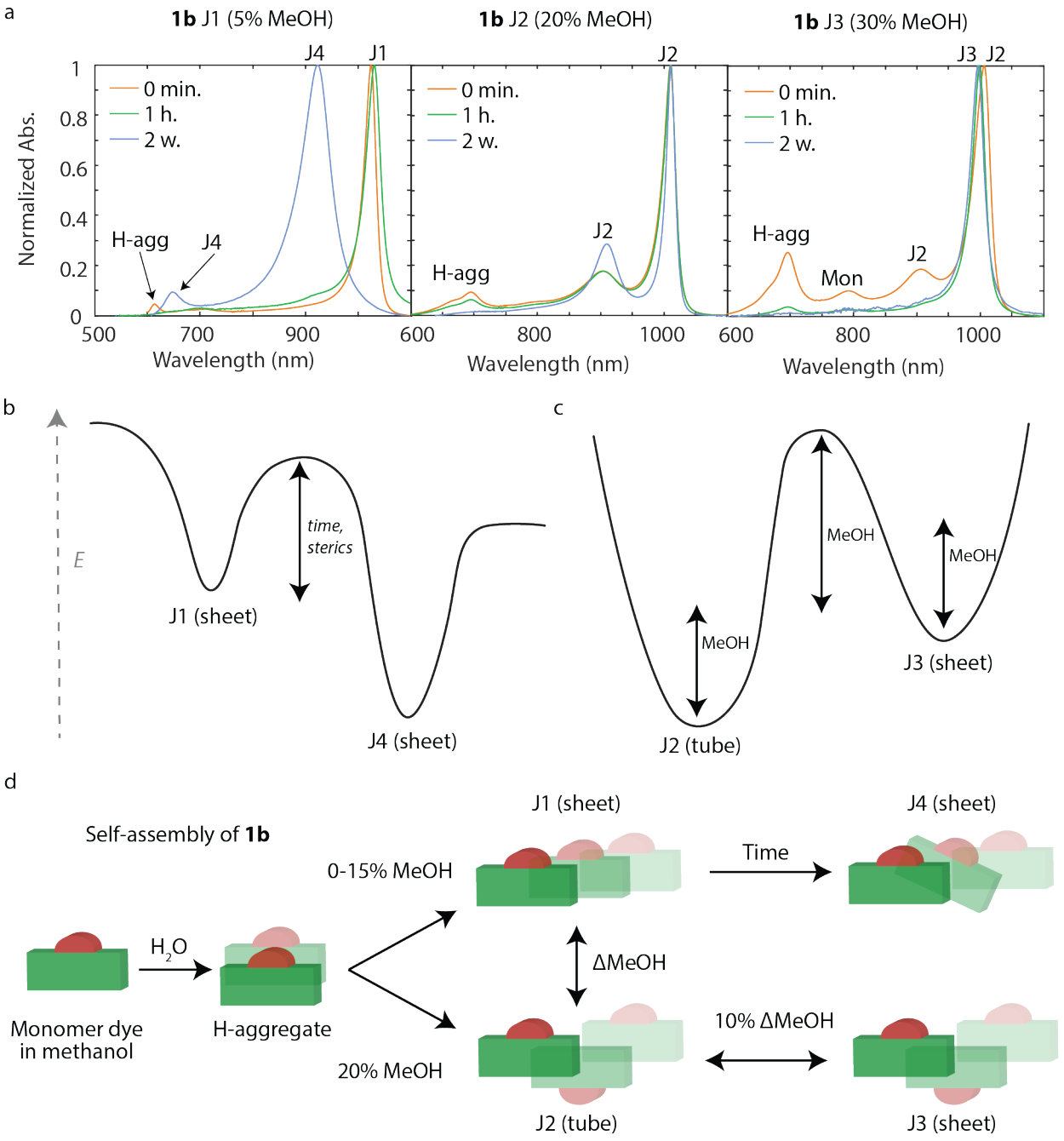

Figure 6. **a)** Absorption profiles of **1b** aggregates under three different preparation conditions (% methanol) after varying aggregation times. **b)** Potential energy diagrams depicting the transition of J1 to J4. **c)** Energy diagram of J2 to J3. **d)** Cartoon depicting self-assembly for aggregates of **1b**.

converting faster. At 5% MeOH, the full J1 to J4 conversion of **1b** occurs over approximately 14 days at room temperature (Figure 3b). The **1b** J2 aggregate (20% MeOH) also initializes with a small amount of H-aggregate, suggesting that the J1 and J2 aggregates are formed directly from an H-aggregate at very early (before 1 s) timepoints. Interestingly, the **1b** J3 (30% MeOH) aggregate initializes in the J2 aggregate, and quickly converts to the fully J3 species over roughly 1 h.

Beyond initialization experiments, we conducted methanol and water dilutions to see how the aggregates of **1b** respond to changing methanol/water ratio. Interestingly, the J1-J3 aggregates display a high degree of interconversion. By diluting the J1 with methanol up to 20 or 30%, we see conversion to the J2 and J3 aggregates, respectively. By diluting the J2 aggregate up to 30% methanol, we observe conversion from J2 to J3. Additionally, dilution of the J3 aggregate (30% MeOH) with water down to 20 and 10% methanol allows for interconversion back to the J2 and J1 aggregates, respectively. Rapid interconversion between J2 (tube) and J3 (sheets) suggests that they share a similar unit cell structure but the mesophase formation depends on the relative solubility difference between 20 and 30% water methanol mixture. Thus the resulting aggregate can be easily tuned by the solvent conditions.

4. Trends in self-assembly across dye structures: Overall, trends between different dye structures allow us to make tentative assignments of underlying structure. Here we focus on the trends in the self-assembly and stability of these aggregates as we change the steric bulk. We found that the J1 aggregates were increasingly unstable as steric bulk increased. For example, the J1 aggregates of **1a** and **1b** are readily isolated at room temperature and convert over weeks (**1a**) to days (**1b**) to the J4 species depending on methanol composition; however, J1 aggregates of **1c** and **1d** were only able to be isolated at lower temperatures (~0-5 °C), meaning they convert

immediately to a different species (J4) upon preparation at room temperature. Additionally, the J1 formed from **1a** and **1b** does not convert, even in small amounts, to J4 at low temperatures (4-8° C) over several weeks. These data imply that the J1 species is a kinetic trap which, if given sufficient activation energy, interconverts to more stable aggregate morphology J4, as opposed to the J3 aggregates, which were stable at room temperature across **1a-d.** Both the steric bulk of the monomer dye and methanol composition seem to affect the energy barrier between J1 and J4 (Figure 6b). Because dyes **1c** and **1d** do not form J1 aggregates at room temperature, we know their barrier between J1 and J4 is much lower. Additionally, because the J1 to J4 interconversion occurs more quickly at high MeOH percentages, we know that the barrier must also be lower. In Figure 6c, we show that the relative energies of the J2 and J3 aggregates and the barrier for interconversion can be adjusted by varying the methanol/water ratio. When methanol is lower (20%), the J2 aggregate is favored, but at higher ratios (30%) the J3 aggregate is favored.

These observations can be connected to potential structural morphological changes. To summarize, the cryo-EM showed us that J1, J3, and J4 share 2D sheet-like morphologies, and that J2 is a single-walled nanotube. Because there are only a small number of ways to pattern the dye monomer such that a single molecule thick 2D sheet organizes from its constituent unit, we began by considering the simplest possible cases of supramolecular organization where each dye has the same orientation, and monomers are slipped from their nearest neighbors. We attribute this structure to the J1 species, which becomes increasingly unstable with steric bulk. We hypothesize that the pendant groups begin to approach each other and therefore push the dyes further apart (leading to redshift). This simple organization allows the dyes to rapidly assemble, though it also explains why the J1 is kinetically disfavored in dyes **1c** and **1d**—the energy penalty of steric clash from their pendant groups becomes large enough that other morphologies (J3 and J4) form

immediately, as opposed to slow conversion over time. In all cases, J1 is a kinetic trap that, while relatively unstable, can organize quickly and slowly find a lower energy conformation over time. Additionally, the AFM reveals that J1 aggregates show the smallest monolayer thickness, which agrees with the proposed structure. DLS also consistently suggests a smaller size for J1, suggesting potentially increased size-dependent strain limiting aggregation. Finally, J1 displays increasing redshift with increased steric bulk compared to J3 and J4 morphologies, suggesting increased slip among monomers results in stronger J-coupling.

We assign the J4 structure to a frustrated, slightly larger, and more disordered morphology that forms from J1. J4 and J1 are connected mesophases showing interconversion over time without methanol. However, we know from AFM that J4 is a thicker monolayer (2.08 vs. 1.34 nm), meaning that some change must occur which widens the monolayer's thickness. For **1a** and **1b**, we see that the J4 aggregate has a secondary, blueshifted peak that photobleaches concurrently with the main peak (Figure S1) we attribute this side feature to an out of plane transition within the 2D sheet; that secondary transition suggests a slightly angled orientation of dye monomers within the extended sheet, depicted in Figure 6d. We note, however, another potential explanation is the appearance of a second peak in **1a** and **1b** J4 may be donor-acceptor coupling as is seen in squaraine J-aggregates. As cyanines contain excited states that follow the donor-acceptor-donor motif described in squaraines, such coupling is possible, though to our knowledge has not been reported for cyanine aggregates.[38,39]

In considering J2 and J3, we hypothesize they feature dyes in a configuration such that nearest neighbors are rotated 180 degrees (i.e. antiparallel) from one another. The formation of single-walled nanotubes in the J2 of **1b** indicates that there are hydrophilic groups (i.e. sulfonates) present on the inner and outer walls of the tube, which would intuitively require the antiparallel

packing. As J3 appears to be a connected mesophase to J2, we expect it to have a similar arrangement. This structural characterization is bolstered by the observation that the J3 aggregates blueshift with increasing steric bulk (Figure 6d); meaning that as the pendant group grows larger, the dyes become less slipped from one another, thereby decreasing the J-coupling (blueshifting). Assuming this alternating packing arrangement, bulkier central groups would cause and decrease in slip because of steric hindrance between neighboring dyes. Additionally, we know that the J3 dyes are thicker than J1 based on AFM (1.62 vs. 1.34 nm) and DLS (600 vs 200 nm) characterizations that show slightly larger monolayers, further suggesting this antiparallel arrangement. The 1d dye was anomalous in the fact that the J3 was discovered to have a larger height than that of the J4 dye. We believe in this case, that the height contribution from the alternating dyes is larger than that of the out-of-plane element attributed to the J4 aggregate.

Conclusion

We synthesized four new cyanine dyes with varying steric bulk in their pendant (4') position and demonstrated that increasing the steric bulk leads to an increased redshift of the dye's J-aggregates. The dyes display rich aggregation behavior, leading to 3-4 J-aggregates with unique spectral signatures that come from different 2D-sheet (one tubular) morphologies despite near identical monomer photophysical properties. We correlate the cryo-electron microscopy to several other structural measurements (AFM, DLS, and kinetic observations) to gain intuition on the structures and hypothesize how different packing arrangements of the monomers yields three unique sheet-like morphologies and one tubular morphology with varying degrees of redshift. In particular, we find the J1 aggregates to be a kinetic trap that slowly interconvert to a blueshifted J4 species, while a J2 aggregate is a single-walled nanotube morphology that shares an anti-parallel

arrangement with the J3 sheets. J4 we tentatively assign to be a larger, more disordered sheet, with some out of plane component.

This work provides several key insights. First, we show generally how minute modifications to a dye monomer structure can lead to extreme changes in the resulting J-aggregate's morphology and photophysics. Second, we observe how the addition of substituents to the 4' position of a cyanine dye is an effective way to induce systematic changes in the chromophore's scaffold without significantly altering solubility or electronic structure. In particular, we maintain that the addition of steric bulk is effective in slipping dyes further apart within a J-aggregate, and therefore modulating the photophysical properties.

Beyond our desire for extramolecular control over photophysical properties, we found clear evidence of distinct morphological phases can form within 2D sheet-like J-aggregates, based on subtle changes in solubility and co-solvent concentrations. Without the clear spectroscopic shifts that arise due to chromphore coupling, these differences would not be observable. Our results thus suggest that one can invert J-aggregate photophysics as a detailed probe of supramolecular structure and kinetics. Thus, we demonstrate that combining photophysical characterization with detailed structural analysis could enable new studies of self-assembly and complexity in supramolecular aggregates.

References

(1) Jelley, E. E. Spectral Absorption and Fluorescence of Dyes in the Molecular State. *Nature* **1936**, No. 138, 1009–1010.

(2) Bricks, J. L.; Slominskii, Y. L.; Panas, I. D.; Demchenko, A. P. Fluorescent J-Aggregates of Cyanine Dyes: Basic Research and Applications Review. *Methods Appl. Fluoresc.* **2018**, *6* (1). https://doi.org/10.1088/2050-6120/aa8d0d.

(3) Deshmukh, A. P.; Koppel, D.; Chuang, C.; Cadena, D. M.; Cao, J.; Caram, J. R. Design Principles for Two-Dimensional Molecular Aggregates Using Kasha's Model: Tunable

Photophysics in near and Short-Wave Infrared. *J. Phys. Chem. C* **2019**, *123* (30), 18702–18710. https://doi.org/10.1021/acs.jpcc.9b05060.

(4) Deshmukh, A. P.; Zheng, W.; Chuang, C.; Bailey, A. D.; Williams, J. A.; Sletten, E. M.; Egelman, E. H.; Caram, J. R. Near-Atomic-Resolution Structure of J-Aggregated Helical Light-Harvesting Nanotubes. *Nat. Chem.* **2024**. https://doi.org/10.1038/s41557-023-01432-6.

(5) Deshmukh, A. P.; Bailey, A. D.; Forte, L. S.; Shen, X.; Geue, N.; Sletten, E. M.; Caram, J. R. Thermodynamic Control over Molecular Aggregate Assembly Enables Tunable Excitonic Properties across the Visible and Near-Infrared. *J. Phys. Chem. Lett.* **2020**, *11* (19), 8026–8033. https://doi.org/10.1021/acs.jpclett.0c02204.

(6) Bailey, A. D.; Deshmukh, A. P.; Bradbury, N. C.; Pengshung, M.; Atallah, T. L.; Williams, J. A.; Barotov, U.; Neuhauser, D.; Sletten, E. M.; Caram, J. R. Exploring the Design of Superradiant J-Aggregates from Amphiphilic Monomer Units. *Nanoscale* **2023**, *15* (8), 3841–3849. https://doi.org/10.1039/d2nr05747f.

(7) Eisele, D. M.; Arias, D. H.; Fu, X.; Bloemsma, E. A.; Steiner, C. P.; Jensen, R. A.; Rebentrost, P.; Eisele, H.; Tokmakoff, A.; Lloyd, S.; Nelson, K. A.; Nicastro, D.; Knoester, J.; Bawendi, M. G. Robust Excitons Inhabit Soft Supramolecular Nanotubes. *Proc. Natl. Acad. Sci. U. S. A.* **2014**, *111* (33), E3367–E3375. https://doi.org/10.1073/pnas.1408342111.

(8) Cosco, E. D.; Arús, B. A.; Spearman, A. L.; Atallah, T. L.; Lim, I.; Leland, O. S.; Caram, J. R.; Bischof, T. S.; Bruns, O. T.; Sletten, E. M. Bright Chromenylium Polymethine Dyes Enable Fast, Four-Color in Vivo Imaging with Shortwave Infrared Detection. *J. Am. Chem. Soc.* **2021**, *143* (18), 6836–6846. https://doi.org/10.1021/jacs.0c11599.

(9) Wang, R.; Huang, T.; Xue, J.; Tong, J.; Zhu, K.; Yang, Y. Prospects for Metal Halide Perovskite-Based Tandem Solar Cells. *Nat. Photonics* **2021**, *15* (6), 411–425. https://doi.org/10.1038/s41566-021-00809-8.

(10) Dang, Z.; Liu, X.; Du, Y.; Wang, Y.; Zhou, D.; Zhang, Y.; Zhu, S. Ultra-Bright Heptamethine Dye Clusters Based on a Self-Adaptive Co-Assembly Strategy for NIR-IIb Biomedical Imaging. *Adv. Mater.* **2023**, *35* (46), 1–15. https://doi.org/10.1002/adma.202306773.

(11) Ou, Y. F.; Ren, T. B.; Yuan, L.; Zhang, X. B. Molecular Design of NIR-II Polymethine Fluorophores for Bioimaging and Biosensing. *Chem. Biomed. Imaging* **2023**, *1* (3), 220–233. https://doi.org/10.1021/cbmi.3c00040.

(12) Ma, X.; Huang, Y.; Li, A.; Zeng, X.; Liu, S. H.; Yin, J.; Yang, G. F. The Aggregates of Near-Infrared Cyanine Dyes in Phototherapy. *ChemMedChem* **2023**, *18* (15). https://doi.org/10.1002/cmdc.202300204.

(13) Sun, C.; Li, B.; Zhao, M.; Wang, S.; Lei, Z.; Lu, L.; Zhang, H.; Feng, L.; Dou, C.; Yin, D.; Xu, H.; Cheng, Y.; Zhang, F. J-Aggregates of Cyanine Dye for NIR-II in Vivo Dynamic Vascular Imaging beyond 1500 Nm. *J. Am. Chem. Soc.* **2019**, *141* (49), 19221–19225. https://doi.org/10.1021/jacs.9b10043.

(14) Zhao, F.; Hu, J.; Guan, D.; Liu, J.; Zhang, X.; Ling, H.; Zhang, Y.; Liu, Q. Boosting Dye-Sensitized Luminescence by Enhanced Short-Range Triplet Energy Transfer. *Adv. Mater.* **2023**, *35* (51), 1–9. https://doi.org/10.1002/adma.202304907.

(15) Jiang, Z.; Ren, A.; Yan, Y.; Yao, J.; Zhao, Y. S. Exciton-Polaritons and Their Bose–Einstein Condensates in Organic Semiconductor Microcavities. *Adv. Mater.* **2022**, *34* (4), 1–25. https://doi.org/10.1002/adma.202106095.

(16) Völker, S. F.; Schmiedel, A.; Holzapfel, M.; Renziehausen, K.; Engel, V.; Lambert, C. Singlet-Singlet Exciton Annihilation in an Exciton-Coupled Squaraine-Squaraine Copolymer: A Model toward Hetero-J-Aggregates. *J. Phys. Chem. C* **2014**, *118* (31), 17467–17482. https://doi.org/10.1021/jp5055809.

(17) Kim, J. H.; Schembri, T.; Bialas, D.; Stolte, M.; Würthner, F. Slip-Stacked J-Aggregate Materials for Organic Solar Cells and Photodetectors. *Adv. Mater.* **2022**, *34* (22). https://doi.org/10.1002/adma.202104678.

(18) Stender, B.; Völker, S. F.; Lambert, C.; Pflaum, J. Optoelectronic Processes in Squaraine Dye-Doped OLEDs for Emission in the near-Infrared. *Adv. Mater.* **2013**, *25* (21), 2943–2947. https://doi.org/10.1002/adma.201204938.

(19) Zampetti, A.; Minotto, A.; Cacialli, F. Near-Infrared (NIR) Organic Light-Emitting Diodes (OLEDs): Challenges and Opportunities. *Adv. Funct. Mater.* **2019**, *29* (21), 1–22. https://doi.org/10.1002/adfm.201807623.

(20) Miao, S.; Liang, Y.; Zhang, Y.; Chen, D.; Wang, X. J. Broadband Short-Wave Infrared Light-Emitting Diodes Based on Cr3+-Doped LiScGeO4Phosphor. *ACS Appl. Mater. Interfaces* **2021**, *13* (30), 36011–36019. https://doi.org/10.1021/acsami.1c10490.

(21) Wang, S.; Chervy, T.; George, J.; Hutchison, J. A.; Genet, C.; Ebbesen, T. W. Quantum Yield of Polariton Emission from Hybrid Light-Matter States. *J. Phys. Chem. Lett.* **2014**, *5* (8), 1433–1439. https://doi.org/10.1021/jz5004439.

(22) Georgiou, K.; Jayaprakash, R.; Lidzey, D. G. Strong Coupling of Organic Dyes Located at the Surface of a Dielectric Slab Microcavity. *J. Phys. Chem. Lett.* **2020**, *11* (22), 9893–9900. https://doi.org/10.1021/acs.jpclett.0c02751.

(23) Nosrati, S.; Rammler, T.; Meixner, A. J.; Wackenhut, F. Combining Optical Strong Mode Coupling with Polaritonic Coupling in a λ/2 Fabry-Pérot Microresonator. *J. Phys. Chem. C* **2021**, *125* (23), 13024–13032. https://doi.org/10.1021/acs.jpcc.1c03004.

(24) Deshmukh, A. P.; Geue, N.; Bradbury, N. C.; Atallah, T. L.; Chuang, C.; Pengshung, M.; Cao, J.; Sletten, E. M.; Neuhauser, D.; Caram, J. R. Bridging the Gap between H- and J-Aggregates: Classification and Supramolecular Tunability for Excitonic Band Structures in Two-Dimensional Molecular Aggregates. *Chem. Phys. Rev.* **2022**, *3* (2). https://doi.org/10.1063/5.0094451.

(25) Friedman, H. C.; Emily, D.; Atallah, T. L.; Jia, S.; Sletten, E. M.; Caram, J. R.; Friedman, H. C.; Cosco, E. D.; Atallah, T. L.; Jia, S.; Sletten, E. M. Establishing Design Principles for Emissive Organic SWIR Chromophores from Energy Gap Laws Establishing Design Principles for Emissive Organic SWIR Chromophores from Energy Gap Laws. *CHEMPR*

7 (12), 3359–3376. https://doi.org/10.1016/j.chempr.2021.09.001.

(26) Arachchi, D. H. T.; Barotov, U.; Perkinson, C. F.; Šverko, T.; Kaplan, A. E. K.; Bawendi, M. G. Bright and Fast Emission from Robust Supramolecular J-Aggregate Nanostructures through Silica-Encapsulation. *ACS Nano* **2024**, *14*, 17. https://doi.org/10.1021/acsnano.4c04732.

(27) Zhu, S.; Tian, R.; Antaris, A. L.; Chen, X.; Dai, H. Near-Infrared-II Molecular Dyes for Cancer Imaging and Surgery. *Adv. Mater.* **2019**, *31* (24), 1–25. https://doi.org/10.1002/adma.201900321.

(28) Pengshung, M.; Li, J.; Mukadum, F.; Lopez, S. A.; Sletten, E. M. Photophysical Tuning of Shortwave Infrared Flavylium Heptamethine Dyes via Substituent Placement. *Org. Lett.* **2020**, *22* (15), 6150–6154. https://doi.org/10.1021/acs.orglett.0c02213.

(29) Zhang, C.; Wu, Y.; Zeng, F.; Wen, Y.; Chen, J.; Deng, G.; Zhang, L.; Zhao, S.; Wu, S.; Zhao, Y. Structurally Modulated Formation of Cyanine J-aggregates with Sharp and Tunable Spectra for Multiplexed Optoacoustic and Fluorescence Bioimaging. *Angew. Chemie Int. Ed.* **2024**, *202406694*. https://doi.org/10.1002/anie.202406694.

(30) Usama, S. M.; Caldwell, D. R.; Shrestha, P.; Luciano, M. P.; Patel, N. L.; Kalen, J. D.; Ivanic, J.; Schnermann, M. J. Modified Norcyanines Enable Ratiometric PH Imaging beyond 1000 Nm. *Biosens. Bioelectron.* **2022**, *217* (June), 114610. https://doi.org/10.1016/j.bios.2022.114610.

(31) Sun, C.; Li, B.; Zhao, M.; Wang, S.; Lei, Z.; Lu, L.; Zhang, H.; Feng, L.; Dou, C.; Yin, D.; Xu, H.; Cheng, Y.; Zhang, F. J-Aggregates of Cyanine Dye for NIR-II in Vivo Dynaimc Vascular Imaging beyond 1500 Nm. **2019**. https://doi.org/10.1021/jacs.9b10043.

(32) Caram, J. R.; Deshmukh, A. P.; Bailey, A. D.; Forte, L. S.; Shen, X.; Geue, N.; Sletten, E. M. Thermodynamic Control over Molecular Aggregate Assembly Enables Tunable Excitonic Properties across the Visible and Near-Infrared. *J. Phys. Chem. Lett.* **2020**, *11* (19), 8026–8033. https://doi.org/10.1021/acs.jpclett.0c02204.

(33) Von Berlepsch, H.; Kirstein, S.; Böttcher, C. Supramolecular Structure of J-Aggregates of a Sulfonate Substituted Amphiphilic Carbocyanine Dye in Solution: Methanol-Induced Ribbon-to-Tubule Transformation. *J. Phys. Chem. B* **2004**, *108* (48), 18725–18733. https://doi.org/10.1021/jp046546f.

(34) Kirstein, S.; Daehne, S. J-Aggregates of Amphiphilic Cyanine Dyes: Self-Organization of Artificial Light Harvesting Complexes. *Int. J. Photoenergy* **2006**, *2006*, 1–21. https://doi.org/10.1155/IJP/2006/20363.

(35) Chuang, C.; Bennett, D. I. G.; Caram, J. R.; Aspuru-Guzik, A.; Bawendi, M. G.; Cao, J. Generalized Kasha's Model: T-Dependent Spectroscopy Reveals Short-Range Structures of 2D Excitonic Systems. *Chem* **2019**, *5* (12), 3135–3150. https://doi.org/10.1016/j.chempr.2019.08.013.

(36) Deshmukh, A. P.; Bailey, A. D.; Forte, L. S.; Shen, X.; Geue, N.; Sletten, E. M.; Caram, J. R. Principles for Self-Assembly of Cyanine Dyes into 2-Dimensional Excitonic Aggregates across the Visible and Near-Infrared. *ChemRxiv* **2020**, No. 2.

https://doi.org/10.26434/chemrxiv.12609398.v1.

(37) Yu, G.; Walker, M.; Wilson, M. R. Atomistic Simulation Studies of Ionic Cyanine Dyes: Self-Assembly and Aggregate Formation in Aqueous Solution. *Phys. Chem. Chem. Phys.* **2021**, *23* (11), 6408–6421. https://doi.org/10.1039/d0cp06205g.

(38) Ohira, S.; Rudra, I.; Schmidt, K.; Barlow, S.; Chung, S. J.; Zhang, Q.; Matichak, J.; Marder, S. R.; Brédas, J. L. Electronic and Vibronic Contributions to Two-Photon Absorption in Donor-Acceptor-Donor Squaraine Chromophores. *Chem. - A Eur. J.* **2008**, *14* (35), 11082–11091. https://doi.org/10.1002/chem.200801055.

(39) Kaczmarek-Kędziera, A.; Żuchowski, P. S.; Kędziera, D. Nature of Intermolecular Interaction in Squaraine Dimers. *Sci. Rep.* **2020**, *10* (1), 1–17. https://doi.org/10.1038/s41598-020-76631-z.